Polymer Chemistry

PAPER

View Article Online
View Journal | View Issue

Cite this: *Polym. Chem.*, 2014, **5**, 5765

Amorphous and crystalline blends from polytyrosine and pyridine-functionalized anthracene: hydrogen-bond interactions, conformations, intramolecular charge transfer and aggregation-induced emission†

Ke-Ying Shih, Yung-Chih Lin, Tai-Shen Hsiao, Shiang-Lin Deng, Shiao-Wei Kuo and Jin-Long Hong*

Received 20th May 2014
Accepted 13th June 2014

DOI: 10.1039/c4py00706a

www.rsc.org/polymers

A new pyridine-terminated fluorophore of (*E*)-4-(2-(anthracen-9-yl)vinyl)pyridine (AnPy) with intramolecular charge transfer (ICT) and aggregation-induced emission (AIE) properties was synthesized and was blended with different amounts of polytyrosine (PTyr) through preferable hydrogen-bond (H-bond) interactions. In blends of a low AnPy content, the rigid PTyr peptide chains serve as templates to H-bond to AnPys, imposing rotational restriction and reinforcing the AIE-related emission intensity of AnPys, resulting in amorphous blends with the observed glass transitions dependent on the composition of the blends. In contrast, when large amounts of AnPys were added, excess AnPys will form new crystals, in between the amorphous regions, constituted of the near parallel dimers of AnPys. With the hampered molecular rotation, the parallel dimers of AnPys in the highly AnPy-loaded blends emit strongly with intensity much higher than those for the amorphous blends. In this study, conformations of the blends and the degree of restricted molecular rotation were assessed in order to correlate with the AIE-related fluorescence behaviour.

Introduction

Considerable efforts to investigate polypeptides have been attempted due to their potential applications in various scientific fields and their close relationship with molecular recognition and proteins.[1–9] Polypeptides can form hierarchically ordered structures containing fundamental secondary structures: α-helices, which can be regarded as rigid rods stabilized through intramolecular hydrogen bond (H-bond) interactions, and β-sheets, stabilized by intermolecular interactions.[10–12] Previously, the secondary structures of the polypeptides poly(γ-methyl-L-glutamate) (PMLG), poly(γ-ethyl-L-glutamate) (PELG), and poly(γ-benzyl-L-glutamate) (PBLG)[13,14] were found to be affected through blending with other random-coil non-peptide oligomers [namely, phenolic resin or poly(vinylphenol) (PVPh)], mediated by H-bond interactions. Polytyrosine (PTyr)[15] was also mixed with poly(4-vinylpyridne) (PVP), through facile H-bond interactions, to prepare interpolymer complexes and miscible blends by applying different solvents in the preparation step. It was found that the content of the secondary structure (basically, the β-sheet conformation) in these blend systems correlated strongly with the strengths of intermolecular H-bonding to the H-bond accepting PVP.

As fluorescence spectroscopy constitutes one of the most powerful tools to study the aggregation of polymers, traditional fluorescent probes such as carbazolyl,[16] dansyl[17] and pyrene[18] have been chemically incorporated with PBLG to monitor the chain conformations of PBLG in solution. For example, poly(ethylene glycol)-*b*-PBLG has been labelled with pyrene[18] and the absence of excimer emission suggested that the pyrene groups were separated from each other in the self-assembled structure. A study on triblock PBLG–polyfluorene–PBLG copolymers[19] suggested that formations of rod–rod–rod and coil–rod–coil conformations are dependent on the solvent casting history and the morphological variations resulted in different FL emission and FL decay behaviours. All previous studies suggested that fluorophore-labelled PBLG is a useful methodology to detect the aggregation behaviour of the PBLG chain.

Traditional planar organic fluorophores generally exhibit weak emission in the aggregated state due to the aggregation-caused quenching (ACQ). In contrast, non-coplanar fluorophores with aggregation-induced emission (AIE) have the unusual enhanced emission in the aggregated state. Since the first discovery in 2001 that the silole derivative[20,21] is an

Department of Materials and Optoelectronic Science, National Sun Yat-Sen University, Kaohsiung 80424, Taiwan, Republic of China. E-mail: jlhong@mail.nsysu.edu.tw; Tel: +886-7-5252000 ext. 4065

† Electronic supplementary information (ESI) available: Fig. S1–S5. See DOI: 10.1039/c4py00706a

AIE-active material, lots of organic and polymeric materials[22–27] have been explored to exhibit the AIE or aggregation-enhanced emission (AEE) properties. It is generally accepted that the restricted intramolecular rotation (IMR) of the phenyl peripheries[28–30] against the central silole core, which reduces the possible nonradiative decay channels and leads to enhanced emission, is the main mechanism responsible for the observed AIE properties. To intensify rotational restriction on the fluorophores, large substituents were frequently used to chemically link with the central core of AIE-active molecules.

Besides using a chemically-linked substituent, the noncovalent H-bond interactions can be also applied to intensify restriction on IMR of the AIE-active fluorophores. The dimer structure of an AIE-active 2,7-bis(4-(*tert*-butylthio)phenyl)-uorenone[31] (BPU) was locked by intermolecular H-bonds and the excited BPU therefore underwent enhanced excimer emissions with fewer non-radiative decays. The salicylideneaniline[32] compound formed a gel in certain organic solvents and its AEE behaviour is ascribed to the formation of J-aggregates and the inhibition of molecular rotation by H-bond interactions in the viscous gel. Several other compounds[33–36] were also reported to show enhanced emission in a gelled state promoted by H-bond interactions. Poly(fluorene-*alt*-naphthol)[37] (PFN) prepared in our laboratory was also found to be AEE-active due to the restricted molecular rotation promoted by inter and intrachain H-bond interactions. Through facile H-bond interactions between PFN and poly(*N*-vinyl pyrrolidone), the resulting PFN/PVR blends[38] showed enhanced emission. The AIE-active fluorophores containing pyridine and triphenylamine functions[39,40] can be also mixed with poly(vinyl phenol) and poly(vinyl alcohol) and the resulting blends all have higher emission intensity than the starting AIE-active fluorophores.

In our laboratory, an AIE-active fluorophore of tetraphenylthiophene (TP) had been incorporated with poly(γ-benzyl-L-glutamate) (PBLG)[41] as terminal and central groups, to prepare TP-1PBLG and TP-2PBLG polymers, respectively. The terminal TP groups in TP-1PBLG can intermolecularly approach each other in the solution aggregated state and therefore exhibited strong solution emission. In contrast, the central TP group, with steric bulkiness imposed by two neighbouring α-helical peptide chains, in TP-2PBLG emitted weakly due to the difficulty to undergo intermolecular aggregation of the TP centers. By adding trifluoroacetic acid (TFA) to dissociate the intramolecular H-bond interactions, the resulting random coil emitted with stronger fluorescence intensity compared to the initial solution of TP-2PBLG. The influence of the secondary structure (specifically, the rigid α-helix structure) on the AEE-related FL behaviour was therefore evaluated.

A convenient noncovalent H-bond interaction, instead of a chemical bond used in TP-1PBLG and TP-2PBLG,[41] is applied in this study to construct a new AIE-active polypeptide (Scheme 1) blend system. Through facile H-bond interactions, polytyrosine (PTyr), with H-bond donating phenol (Ph) pendant groups, serves as an effective template capable of reacting large amounts of AIE-active fluorophores of (*E*)-4-(2-(anthracen-9-yl)vinyl)pyridine (AnPy) with a H-bond accepting pyridine (Py) terminal, to result in different AnPy/PTyr

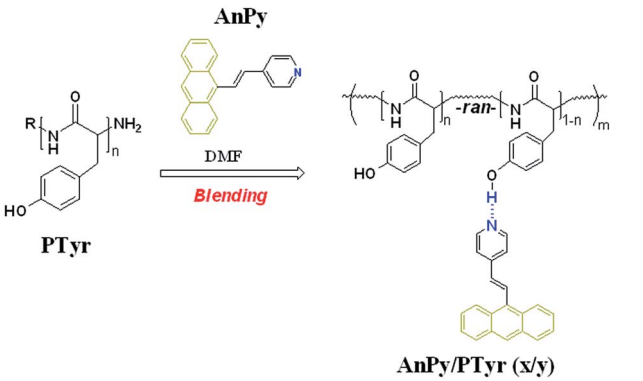

Scheme 1 Synthesis of AnPy by Heck coupling reaction and preparation of AnPy/PTyr (*x*/*y*) blends through H-bond interactions between the pyridine ring of AnPy and the phenolic OH group of PTyr.

(*x*/*y*) (*x*/*y*: molar ratio between Py and Ph functions) blends. With increasing AnPy content, the blends undergo conformation change on both PTyr and AnPy components. The conformation change results in varied degree of restricted IMR,[28–30] as the main mechanism responsible for AIE activity, on the fluorescent AnPy and significantly alters the emission behaviour of the blends. Conformation change involved in PTyr and AnPy components depends on the amount of AnPy added in the blends. Initially, implantation of AnPy converted the secondary structure of the PTyr peptide chains to a more rigid α-helical structure, which imposes efficient rotational restriction on AnPy, resulting in emission enhancement of the blends. Later, when large amounts ($x/y > 1$) of AnPys were used, excess AnPys formed new intimately packed crystals, within them the molecular rotation of AnPys is so efficiently restricted that the corresponding crystalline blends emitted with an intensity much higher than the blends with a lower AnPy content. Through different instrumental analyses, the conformation change of the AnPy/PTyr (*x*/*y*) blends was characterized and its relationship with the restricted IMR and the AIE-related emission behaviour were therefore assessed in this study.

Experimental

Materials

L-Tyrosine (MP Biomedicals), triphosgene (TCI), (Acros, 99%), and bromoanthracene (Aldrich) were purchased commercially. All reaction solvents were distilled from an appropriate drying agent prior to use. Polytyrosine (PTyr) was synthesized according to the reported procedure[15,42] (Fig. S1, ESI†). The low MW PTyr oligomer has $M_n = 1419$ and $M_w = 1558$ (Fig. S2, ESI†) according to the result from MALDI-TOF mass spectroscopy. DMF solutions containing calculated amounts of PTyr and AnPy were stirred for 6 h and then the solvent was evaporated slowly at 50 °C for 1 day. Final solid blends were obtained after further drying at 80 °C for 2 days. AnPy was prepared from the Heck-coupling reaction and is detailed below: (Scheme S1†).

Synthesis of 4-[2-(9-anthryl)vinyl]pyridine (AnPy)

Reaction mixtures of 4-vinylpyridine (1.65 ml, 14.88 mmol), 9-bromoanthracene (5.00 g, 19.44 mmol), triethylamine (2 ml), $Pd(OAc)_2$ (0.17 g, 0.73 mmol) and tri-*o*-tolylphosphine (0.11 g, 0.36 mmol) in dry DMF (80 ml) were thoroughly mixed under argon. The reaction mixtures were then degassed by free-pump-thaw for 5 times before heating at 120 °C for 18 h. After cooled to room temperature, the reaction mixtures were poured into water and the resultant suspensions were extracted with CH_2Cl_2 (3 × 50 ml). The combined organic extracts were washed with brine, dried over $MgSO_4$ and concentrated by a rotary evaporator. The crude product was then purified by column chromatography (v/v hexane/ethyl acetate = 5/5) to give 1.51 g (27.5% yield) of yellow AnPy as the final product. ^{1}H NMR (500 MHz, $CDCl_3$) δ 8.69–8.67 (d, 2H, H_a), 8.43 (s, 1H, H_i), 8.30–8.25 (d, 2H, H_e), 8.17–8.11 (d, 1H, H_c), 8.05–8.00 (d, 2H, H_h), 7.53–7.46 (m, 6H, $H_{b,f,g}$), 6.92–6.87 (d, 1H, H_d). (Fig. S3, ESI†) ^{13}C NMR (125 MHz, $CDCl_3$): δ 150.8, 145.2, 135.3, 132.1, 131.7, 130.7, 130.2, 129.4, 128, 126.5, 126.1, 125.9, 121.5. (Fig. S4, ESI†); MS *m*/*z*: found, 282.1; anal. calcd for $C_{21}H_{15}N$: C, 89.65; H, 5.37; N, 4.98. Found: C, 89.56; H, 5.82; N, 4.62%.

Characterization

Proton nuclear magnetic resonance (^{1}H NMR) spectra were measured at room temperature using a Bruker AM 500 (500 MHz) spectrometer, with the residual proton resonance of the deuterated solvent used as the internal standard. ^{13}C CP-MAS NMR spectra were acquired on a Bruker 14.1 T wide-bore Avance III spectrometer equipped with a 4 mm double-resonance magic-angle-spinning (MAS) probe head. The Larmor frequency for ^{13}C is 150.92 MHz. The samples were spun at 12 kHz. A wide-angle X-ray diffraction (WAXD) pattern was obtained from a Siemens D5000 X-ray diffractometer with a source of Cu Kα (l¼ 0.154 nm) radiation at 40 kV and 30 mA. Diffraction patterns were collected with a scan rate of 3 s per 0.1° in the 2θ ranges of 2–40°. Mass spectra were recorded using a Bruker Daltonics Autoflex MALDI-TOF mass spectrometer. DSC was performed using a TA-Q20 instrument operated at a scan rate of 20 °C min^{-1} under nitrogen atmosphere. Fourier-transform infrared (FTIR) spectra of the blends were recorded using a Bruker Tensor 27 FTIR spectrophotometer and the conventional KBr disk method. Because polymers containing OH groups are hygroscopic, pure N_2 gas was used to purge the optical box of the spectrometer to ensure dry samples. The emission spectra were obtained from a LabGuide X350 fluorescence spectrophotometer using a 450 W Xe lamp as the continuous light source. Ultraviolet-visible (UV-vis) absorption spectra were recorded with an Ocean Optics DT 1000 CE 376 spectrophotometer. A quartz cell with dimensions of 0.2 × 1.0 × 4.5 cm^3 was used for the UV-vis absorption and the emission spectra measurements. Quantum efficiency (Φ_F) of the solid samples were measured in an integrating sphere made by Ocean Optics.

Results and discussion

The AIE-active fluorophore AnPy was synthesized from Heck coupling reaction between 9-bromoanthracence and vinylpyridine, and its pyridine terminal functioned as H-bond accepting function to react with H-bond donating phenolic OH of PTyr (Scheme 1). With the facile H-bond interactions between AnPy and PTyr, different AnPy/PTyr (*x*/*y*) blends were prepared and characterized. In blends containing small amounts (*x*/*y* < 5/5) of AnPys, the secondary structure of the PTyr peptide chain controlled the AIE-activity of the AnPy molecules. For blends containing excess AnPys, a new crystalline phase enriched with AnPy molecules formed to contribute to the observed intense fluorescence. To have logical discussion, the complicated blend system will be presented in the text after the AIE activity of the new AnPy fluorophore was clarified.

AIE property of AnPy

Fluorescence responses toward concentration and aggregation can be used to characterize the AIE effect of AnPy. Primarily, the effect of concentration was emphasized by the unnormalized PL emission spectra in Fig. 1A, which showed the continuous

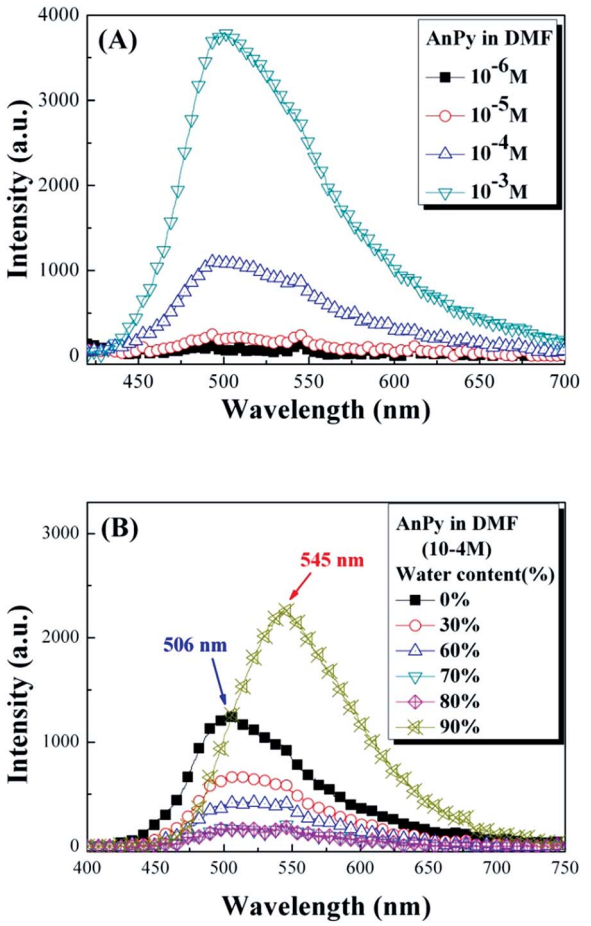

Fig. 1 Solution emission spectra of (A) AnPy in DMF of various concentrations and (B) AnPy (10^{-4} M) in DMF–water mixtures of various compositions (excited at 400 nm).

accession of emission intensity gains with increasing concentration from 10^{-6} to 10^{-3} M. As solution thickening often quenches fluorophore's emission, AnPy solutions nevertheless become more emissive in more concentrated solutions. This peculiar phenomenon of concentration-enhanced emission is due to the AIE effect and more discussion will be given next. Here, although fluorescence of the dilute solution (10^{-6} and 10^{-5} M) is quite weak, two discernible peaks at 506 and 545 nm, attributing to the respective monomer and excimer emissions, are still visible in the spectrum. With increasing concentration, the long-wavelength excimer emission gained its contribution to the whole emission and became a shoulder-like peak buried in the main emission background.

As non-solvent for AnPy, water can be used to generate aggregates from dilute solution and the accompanying fluorescence responses (Fig. 1B) were used to characterize the AIE effect. However, unexpected spectral variations occurred initially since we observed the emission reduction when the water contents are in the ranges from 30 and 80 vol%. The initial emission reduction, accompanied by the bathochromic shift of the emission band, is due to the intramolecular charge transfer (ICT),[43,23] promoted by the polar water included in the solution mixtures, of the excited AnPy species in the polar solvent media. As a polar molecule, solutions of AnPy exhibits a continuous bathochromic shift (Fig. S5, ESI†) and emission reduction in solvents of increasing polarity. In any case, the expected emission enhancement was finally observed in the solution containing 90 vol% of water. The excimer emission at 545 nm is essentially different from other spectra and is more intense than the pure dilute solution of AnPy. The molecular rotation of the AnPy molecules in the water-induced aggregates was effectively restricted, contributing to the intense excimer emission at 545 nm. AnPy is therefore an AIE-active fluorophore and was used as a component to prepare AnPy/PTyr (x/y) blends for further study.

Solution emission of the AnPy/PTyr (5/5) mixtures

The condition of AnPy molecules and PTyr chains being already inter-reacted in the preparative solution state needs to be certified before entering discussion on the solid blends. By keeping the concentration of AnPy in DMF at a constant value of 10^{-4} M, the solution emission intensity (Fig. 2) was progressively increased with increasing PTyr content in the solutions. The emission intensity of the AnPy/PTyr (1/9) mixture is almost three times to that of the pure AnPy solution. While the concentration of the fluorescent AnPy was kept constant in the solutions, the progressive emission gain should be attributed to the continuous influence from the added PTyrs; in this case, the facile H-bond interaction between AnPy and PTyr is the like source contributing to the observed emission responses in Fig. 2. Meaning, when AnPys are H-bonded to the rigid PTyr chains in the solution, the molecular rotation of AnPys was effectively restricted.

To demonstrate the AIE character of the AnPy/PTyr solution mixture, a particular composition of AnPy/PTyr (5/5) was used. Again, the AIE property of the AnPy/PTyr (5/5) mixture can be

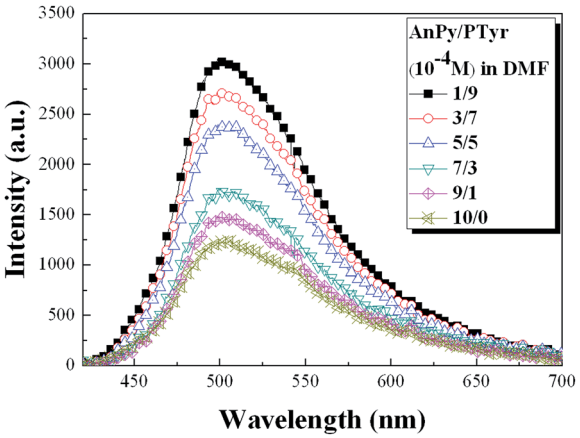

Fig. 2 Solution emission spectra of AnPy (10^{-4} M) in the presence of different molar ratios of PTyr.

evaluated from the spectral responses toward concentration and aggregation. The effect of concentration is emphasized by the unnormalized solution emission spectra of AnPy/PTyr (5/5) in DMF (Fig. 3A), which exhibited the large intensity gain when the concentrations of AnPy and PTyr were both increased from

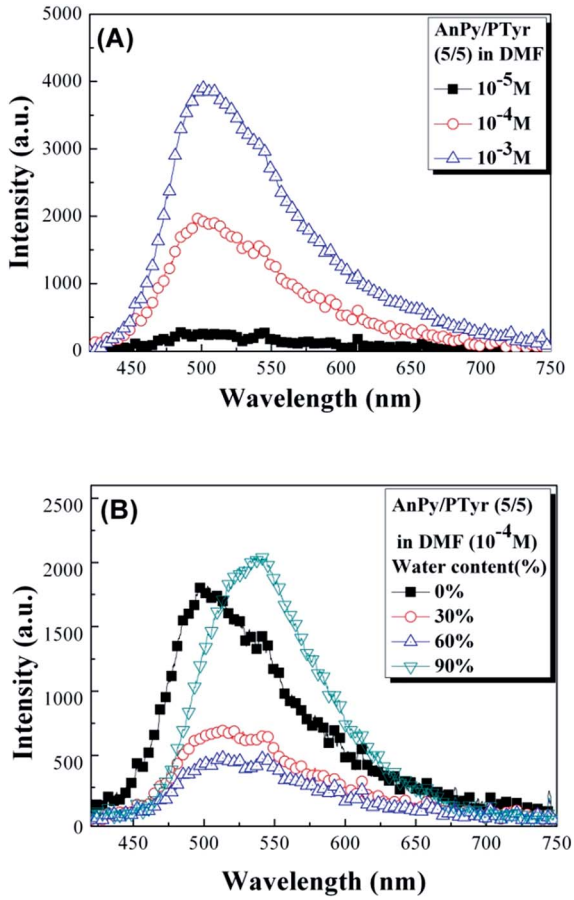

Fig. 3 Solution emission spectra of AnPy/PTyr (5/5) mixtures in (A) DMF of various concentrations and in (B) DMF–water mixtures of various compositions (excited at 400 nm).

10^{-5} to 10^{-3} M. Enhanced molecular contacts in more concentrated solutions generated more H-bonded AnPys in the concentrated solutions, leading to the intense emissions observed in Fig. 3A. The H-bond interaction is therefore effective in imposing restricted molecular rotation on the H-bonded AnPys in the solution mixtures.

Aggregate formation due to non-solvent inclusion is also practiced here to demonstrate the AIE property. As a non-solvent for both AnPy and PTyr, water was used to generate aggregates of the AnPy/PTyr mixtures. Nevertheless, similar to emission of pure AnPy solutions (Fig. 1B), the ICT process was also involved in the initial emission behaviour of the AnPy/PTyr (5/5) solution mixtures; therefore, the initial increase of water content from 30 to 80 vol% resulted in the decrease of emission intensity (Fig. 3B). Nevertheless, emission enhancement was eventually resolved in the solution containing a high fraction (90 vol%) of water. By accepting the premise that certain H-bond interactions should prevail in the solution mixtures (according to Fig. 2), the emission enhancement of the 90 vol% water solution should be attributed to the AIE activity of the H-bonded AnPy molecules in the solution. Here, we also noticed the discernible excimer emission at 545 nm, which are present in all spectra and is the major emission process for the 90 vol% water solution.

Solid emission of the AnPy and AnPy/PTyr blends

Solid AnPy and AnPy/PTyr (x/y) blends cast from the corresponding DMF solutions were prepared and their emission spectra (Fig. 4) were measured. All the solid samples emit with higher intensity than the solution counterparts (*cf.* Fig. 2). The molecular motion of the fluorophores is more effectively restricted in the solid state compared to the mobile solution state. Intense solid emission is therefore resolved in the solid spectra due to the effective rotational restriction. With a low AnPy content, the AnPy/PTyr (1/9) blend emitted with lower intensity than the pure AnPy but increasing AnPy content from 10 to 90 mol% raised the solid emissions. With less AnPy content than the pure AnPy solid, most of the AnPy/PTyr blends emit with higher intensities than the pure AnPy, reflecting that restricted molecular rotation rather than the amounts of the fluorophores is the key factor controlling the AIE-related emission behaviour. When the AnPy content was increased from 10 to 70 mol%, the corresponding emission spectra progressively shifted to lower wavelengths but for the spectrum of AnPy/PTyr (9/1) a reverse bathochromic shift from 506 to 545 nm was observed. The shifting of the emission maxima may reflect the change of the molecular arrangements of the AnPy molecules in the blends and we will discuss it later.

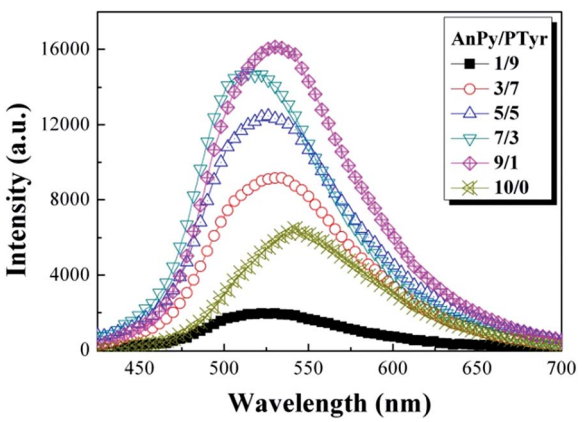

Fig. 4 Solid emission spectra of AnPy and AnPy/PTyr (x/y) blends (excited at 400 nm).

Table 1 summarized the quantum efficiency (Φ_F) of the solid AnPy and AnPy/PTyr (x/y) measured from the integrating sphere. As consistent with the emission spectra in Fig. 4, the emission efficiency of the blends is increased with increasing AnPy content in the blends. The AnPy/PTyr (1/9) blend has the lowest Φ_F of 8% while the AnPy/PTyr (9/1) blend is the highly emissive sample with a Φ_F value of 30%, which is higher than that (18%) of the pure AnPy.

Secondary structures of the AnPy/PTyr blends

DSC is a convenient method for evaluating the thermal characteristics that arise from phase change of the blends.

Generally, only a single glass transition (T_g) can be observed if the components of blends are macroscopically miscible. Blends containing less amounts of AnPy ($x/y < 1$) are therefore homogeneous since only single glass transition (Fig 5) was observed in the thermograms. The macroscopic miscibility in the blends is basically attributed to the effective H-bond interaction between AnPy and PTyr. The resolved T_gs continuously shifted to lower temperatures as the content of the low MW AnPy was further increased. For the AnPy/PTyr (7/3) and (9/1) blends containing excess AnPys, an extra crystalline melting endotherm was observed at temperature close to melting of the pure AnPy. Suggestively, excess non-bonded AnPys in AnPy/PTyr (7/3) and (9/1) started to form a new crystalline phase besides the amorphous H-bonded AnPy/PTyr phase. A co-existing crystalline phase, representative of the pure AnPy molecules, and amorphous phase, representative of the H-bonded AnPy/PTyr species, mainly exist in the highly AnPy-loaded blends. The phase behaviour of the highly AnPy-loaded blends therefore contributes to the distinct fluorescence behaviour.

FTIR spectroscopy can provide information about H-bond interactions between AnPy and PTyr and the secondary structures of polypeptides.[44,45] Pure AnPy provided a characteristic band at 988 cm^{-1}, corresponding to the free pyridine rings while pure PTyr provided a well-separated band at 1013 cm^{-1}

Table 1 Quantum yield (Φ_F)[a] and crystallinity[b] of the solid AnPy and AnPy/PTyr (x/y) blends

x/y =	0/10	1/9	3/7	5/5	7/3	9/1	10/0
Φ_F (%)	—	8.0	19.2	23.4	26.6	30.1	18.0
Crystallinity (%)	37.4	34.7	31.4	37.0	48.3	53.6	80.5

[a] Quantum yield, obtained from the integrating sphere. [b] Evaluated from WAXD in Fig. 10.

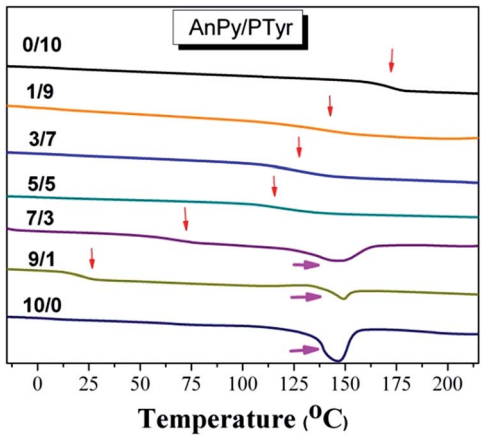

Fig. 5 DSC traces of AnPy, PTyr and AnPy/PTyr (*x*/*y*) blends (heating rate = 20 °C min^{-1}).

due to the pendant phenol absorption. However, this phenol absorption was overlapped with the H-bonded pyridine ring[46,47] at 1005 cm^{-1}. The overlapped absorptions were then deconvoluted by a series of Gaussian distribution (*cf.* the dashed lines in Fig. 6A). The peak areas of the free and H-bonded pyridine absorptions were then resolved and illustrated in Fig. 6B. The fraction of the H-bonded pyridine ring increases monotonically with increasing PTyr content in the blends. This result suggests that the PTyr chain serves as an effective template to build in AnPys in the blends.

Infrared spectra recorded in the ranges from 1720 to 1580 cm^{-1} (Fig. 7) provide information regarding the secondary structures (amide I group) of PTyr and the AnPy/PTyr blends. After analyzing these spectra using the second-derivative technique,[48] the broad absorption pattern observed for pure PTyr covers eight major peaks: for the ring vibrations of tyrosine at 1597 and 1615 cm^{-1}; the α-helical conformation at 1655 cm^{-1}; the β-sheet conformation at 1630 cm^{-1}; the β-turn conformation at 1670 cm^{-1}; and the random coil conformation at 1643, 1683, and 1700 cm^{-1}.[49] Besides the peptide absorption, the aromatic phenyl rings of AnPy also lead to certain absorption bands at 1590, 1620 and 1635 cm^{-1}, respectively; therefore, absorptions from the AnPy component need to be subtracted from the overlapped regions when de-convolution procedures were conducted to resolve the infrared absorptions in the

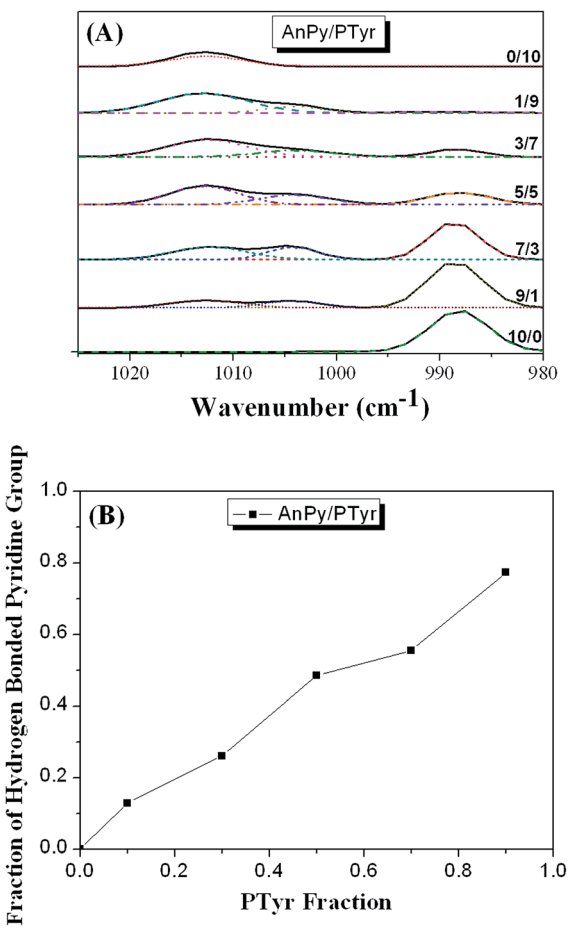

Fig. 6 (A) FTIR spectra of AnPy, PTyr and AnPy/PTyr (*x*/*y*) blends in the region between 1025 and 980 cm^{-1} and (B) the area fraction of H-bonded pyridine rings of AnPy with respect to the PTyr content in the blends.

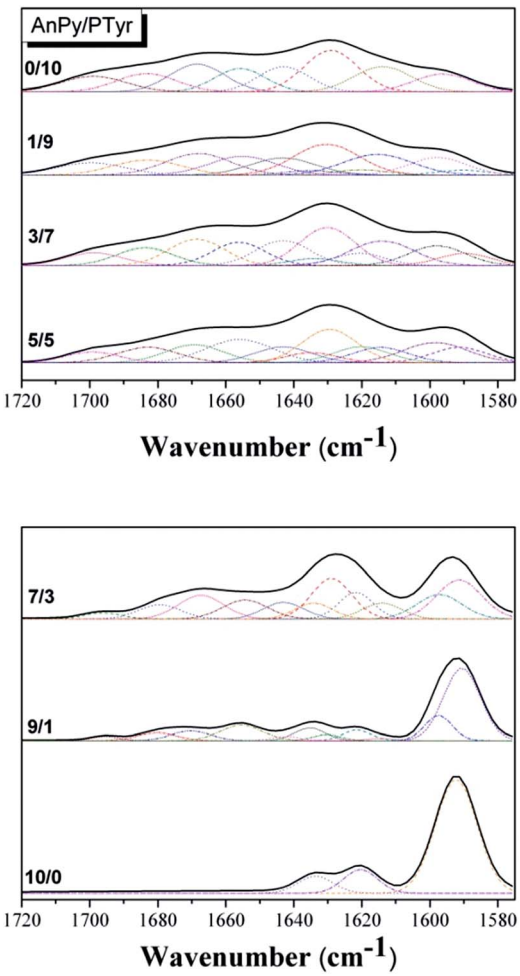

Fig. 7 FTIR spectra and the deconvoluted curves (in dashed line) of AnPy, PTyr and AnPy/PTyr blends in the region between 1720 and 1580 cm^{-1}.

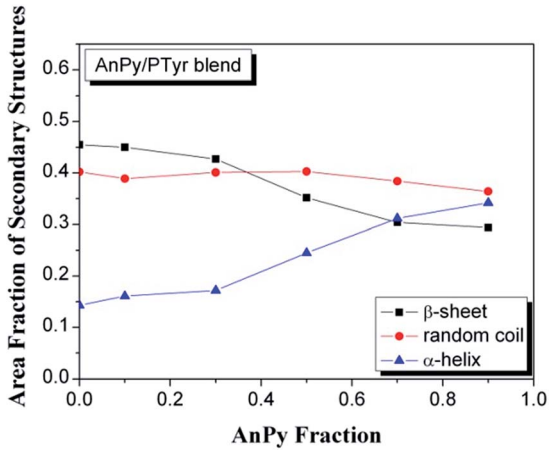

Fig. 8 area fraction of the secondary structures of the AnPy/PTyr blends calculated from the curve-fitting results of Fig. 7.

ranges from 1720 to 1580 cm^{-1}. Fig. 8 summarizes the results from the curve-fitting data for the amide I groups of the β-sheet, α-helical, and random coil structures of PTyr in the presence of different amounts of AnPys. It has been reported that the α-helix and β-sheet secondary structures of PBLG are both present at low DPs (<18), but when the DP increases, the α-helical secondary structure is favored.[10] In this study, both the α-helix and β-sheet conformations are present in the PTyr oligomer at a DP of 8. Initially, fractions of the secondary structure in the AnPy/PTyr (1/9) and (3/7) blends are similar to those of pure PTyr. However, fraction of the α-helical conformation started to rise, at the sacrifice of the β-sheet conformation, with increasing AnPy content in the blends. Meanwhile, the content of the random coil structure remains approximately the same for all AnPy/PTyr blends, reflecting the fact that adding AnPy affects little on the content of the flexible random coil.

Conversion of β-sheet to α-helix structures can be also detected by the ^{13}C CP/MAS NMR spectra (Fig. 9A). The different ^{13}C chemical shifts of the C_α, C_β, and amide C=O carbon atom nuclei relate to the local conformations of the individual amino acid residues, characterized by their dihedral angles and types of intermolecular and intramolecular H-bonds.[50,51] In the case of pure PTyr, the phenolic groups in the side chains could stabilize the α-helical secondary structures; the chemical shifts of the corresponding C_α, C_β, and amide C=O carbon atom nuclei appeared at 58.0, 36.1, and 175.0 ppm, respectively. In the β-sheet conformation, these chemical shifts (52.1, 39.3, and 169.6 ppm, respectively) were located upfield by approximately 3–7 ppm relative to those for the α-helical conformations.[51] The C=O region of the spectrum of the AnPy/PTyr blend system reveals that the contents of the α-helical and β-sheet conformations of PTyr are strongly dependent on the AnPy content in the blends. We thereby conducted deconvolution (Fig. 9B) on the C=O absorptions in the range from 166 to 178 ppm and the result coincides with the finding from the FTIR spectra that the fraction of α-helical conformation increases upon increasing the AnPy content in the AnPy/PTyr blends.

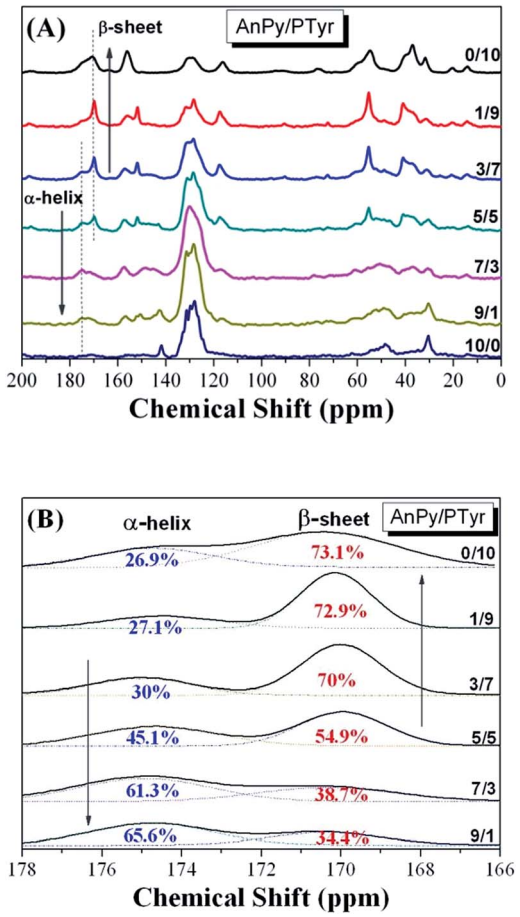

Fig. 9 (A) ^{13}C CPMAS NMR spectra and (B) curve fitting of the signals for AnPy, PTyr and AnPy/PTyr blends in the range from 166 to 178 ppm.

Molecular arrangement of the crystalline AnPys in the blends

WAXD analysis provides information regarding the molecular arrangement of the crystalline AnPy in the blends. Fig. 10 displays the WAXD patterns of AnPy, PTyr and the AnPy/PTyr (*x*/*y*) blends recorded at room temperature. The crystalline nature of pure AnPy is clearly illustrated by the sharp diffraction

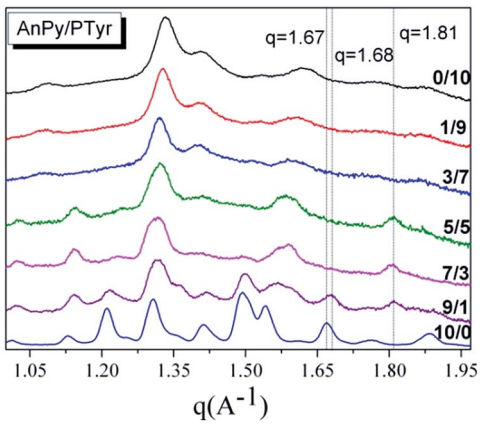

Fig. 10 WAXD patterns of the AnPy/PTyr blends.

peaks and the resolved crystallinity of 80.5% (Table 1). In contrast, the spectrum of PTyr mainly consists of few broad diffraction peaks over the large amorphous background, which results in the low crystallinity of 37.4%. For blends ($x/y < 1$) containing less amounts of AnPys, the presence of crystalline AnPys causes the slight decrease of the crystallinity; however, excess AnPys in the AnPy/PTyr (7/3) and (9/1) blends obviously form new crystals with high crystallinity. A highest crystallinity of 53.6% can be resolved for AnPy/PTyr (9/1). Diffractions in the ranges from $q = 1.0$ to 2.0 can be used to locate the intermolecular distances between the closely packed aromatic rings in the crystalline phase. In this area, diffraction peaks of the blends are overlapped with those of the pure AnPy and PTyr, however, a careful examination still reveals that the interaromatic distances of the blends are shorter than those involved in pure AnPy. The short interaromatic distances of the blends are indicative of intimately packed crystalline lattices, which will impose strong molecular restriction on the crystalline AnPys and thus, rendering in the observed enhanced emission.

The most noticeable feature in Fig. 10 is the new diffraction peaks at $q = 1.807$, which appeared in the spectra of the AnPy/PTyr (5/5), (7/3) and (9/1) blends. The diffraction at $q = 1.81$, essentially at a position different from that for pure AnPy, corresponds to a short diffraction distance of 3.47 Å. A near parallel anthracene–anthracene pair in the AnPy dimer is the like source responsible for this new diffraction. The dimer with such a short inter-anthracene distance has an intimately packed geometry, within which molecular rotation is highly hindered to result in enhanced emission as observed in Fig. 4. Upon photoirradiation, the excited dimer preserves the intimately packed geometry, which relaxes, with reduced non-radiative decay pathways, resulting in the strong excimer emission.

The relative broadness of the diffraction peaks can be used to evaluate the crystal sizes of the newly formed crystals in the highly AnPy-loaded blends ($x/y > 1$). In practice, the Scherrer equation was applied to selected diffraction peaks representative of potential new crystals. For the blends of AnPy/PTyr (5/5), (7/3) and (9/1), the average crystal sizes calculated from the diffraction peaks at $q = 1.81$ is 9.94 nm. For AnPy/PTyr (9/1), the average crystal size from the unique diffraction at $q = 1.677$ is 9.44 nm. Comparatively, the average crystal size of pure AnPy, evaluated from the diffraction at $q = 1.67$ is 17.6 nm, which is larger than those evaluated from the blend samples. It is envisaged that the implanted AnPys in the blends are mostly located in the intermediate regions between the PTyr templates, forming small crystals with the steric constraint imposed by the rigid PTyrs.

Conformation change and the AIE-related emission behaviour

The conformation change upon increasing the AnPy content in the AnPy/PTyr blends is schematically illustrated in Scheme 2. The results from DSC thermograms indicate the presence of two phases in the blends, therefore, an amorphous phase, representative of the aggregated H-bonded PTyr chains, and a crystalline phase, representative of small-mass AnPy molecules, are the fundamental structures involved in the transformation. The aggregated PTyr chains, involved in blends of a low AnPy content ($x/y < 1$), serve as templates for the implanted AnPy molecules, which form H-bonds with the PTyr chains in various orientations, resulting in the formation of an amorphous zone in the interface region, according to the spatial arrangement of the phenol rings in the peptide chains. The H-bonded AnPy molecules in the amorphous zone can be either in the monomeric or in the dimeric form depending on the AnPy content.

The step I in Scheme 2 mainly illustrates the changes of the secondary structure of the aggregated peptide chains under the reaction of the incoming AnPys. Pure PTyr contains both the α-helical and β-sheet structures but the implanted AnPys transform certain β-sheets into the rigid α-helix according to the results from FTIR and ^{13}C CP-MAS NMR. It was then envisaged that the large AnPy molecules act to open the intimately packed β-sheet and convert the peptide segments into the α-helical chains (step I) containing distant phenol pendant groups to accommodate the incoming AnPys.

Step I therefore illustrates the conformation change involved in the blends of low AnPy content ($x/y < 1$). The fundamental feature in the blends can be best illustrated by the coexisting peptide aggregates and the amorphous zone in between the peptide aggregates. Over the surface regions of the peptide aggregates, the H-bonded AnPy monomers are anchored to the peptide chains and are sluggish in rotation with the steric constraint imposed by the rigid PTyr chains. Continuous loading of AnPys generate the amorphous zone, within which AnPys may exist in the forms of monomers and dimers. The increasing crowdedness in the amorphous zone forces AnPys to adopt a less planar geometry emitting at short-wavelength regions. Compared to monomeric AnPys, the dimeric AnPys are more effective emitters in view that the coherent rotation motion of the anthracene–anthracene pair required more energy than the rotation of the monomeric AnPy. The possibility of dimer formation increases with increasing AnPy content in the blends; therefore, emission efficiency of the amorphous blends increases with the increasing AnPy content in the blends. Monomers and dimers in the amorphous zone are therefore responsible for the monomer and excimer emissions observed in the amorphous AnPy/PTyr blends.

Step II, involved in the highly AnPy-loaded blends ($x/y \geq 1$), basically illustrates two features, the reduction on the particle size of the peptide aggregates and the formation of new AnPy crystals. In the blends, large amounts of AnPys act to disperse the large amorphous aggregates into small ones with more surface areas to accommodate excess AnPys. The reduced aggregate dimension with an increasing AnPy content is reflected by the continuous lowering of the glass transition in Fig. 5. Excess AnPys in the blends also form new crystals with shorter intermolecular distances than those in the pure AnPy. In the interface region of the amorphous zone, the initial AnPy–AnPy dimers are randomly distributed over the surfaces of the aggregated peptide chains. However, more parallel dimers in more intimately packed geometry gradually develop, through stepwise adjustments on the orientation of the dimers, along the axis from the amorphous zone to the middle region between the amorphous zones. The intimately packed dimers of varied

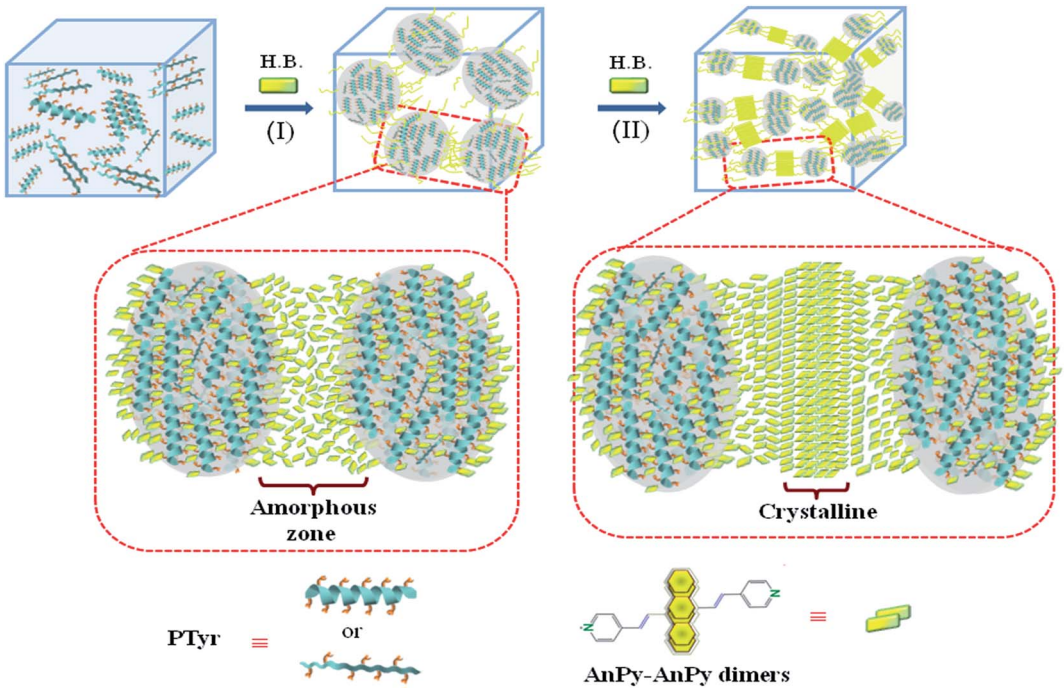

Scheme 2 Steps I and II involved in the conformation change of the AnPy/PTyr (*x*/*y*) blends.

orientations result in different intermolecular distances as reflected by the various diffraction peaks resolve in the WAXD spectra of the blends. In the middle regions between two amorphous PTyr aggregates, the AnPy dimers are considered to adopt the near parallel geometry with an average interanthracene distance of 3.47 Å (at $q = 1.81$). The near parallel dimers are therefore the major feature in the crystalline AnPy/PTyr (9/1) and are responsible for its high excimer emission at 545 nm (Fig. 4). Besides the anticipated hindered rotation of this near parallel dimer, the high crystallinity and the corresponding crystallization-induced emission (CIE)[52,53] is also the key factor contributing to the superior emission intensity of the AnPy/PTyr (9/1) blend. In contrast to the amorphous zone, the crystalline lattices contain less defects and molecular voids and therefore, the near parallel AnPy dimers are firmly fastened, resulting in intense fluorescence due to the blockage of non-radiative decay pathways, in the crystalline lattices. The reinforced rotational restriction is again the controlling factor leading to the high emission of the crystalline blends.

Conclusions

The organic fluorophore of AnPy was synthesized and characterized to have the interesting ICT-AIE characters by its solution emission responses toward concentration and aggregation. The terminal pyridine ring of AnPy can be used as a H-bond donating group to react with a H-bond accepting phenolic OH group of PTyr. Through facile H-bond interactions, amorphous and crystalline AnPy/PTyr (*x*/*y*) blends of varied compositions can be prepared and characterized.

Facile H-bond interactions between AnPy and PTyr should already take place in the dilute solution state since the solution emission of AnPy was enhanced by increasing the PTyr content in the solution. The H-bonded AnPys are also AIE-active materials according to the solution emission behaviour of the AnPy and PTyr mixtures. The concentration and aggregate formation all resulted in enhanced emission of the solution mixture. After removal of the solvent, the resulting AnPy/PTyr (*x*/*y*) solid blends are highly emissive materials with the emission intensity increasing with the AnPy content. Spectral analysis indicated that the loading of AnPys transformed the β-sheet conformation into a rigid α-helix form; at the same time, the initial amorphous blends were converted into two-phase materials containing an extra crystalline phase constituted by the intimately packed dimers of AnPy. In the amorphous blends, the rigid PTyr templates preferably bond and impose rotational restriction to AnPys, resulting in enhanced emission of the AnPy component. In the highly AnPy-loaded blends, excess AnPys form a new crystalline phase, constituted by intimately packed dimers of AnPy, in between the amorphous regions. The intimately packed dimers in the crystalline regions are sluggish in molecular rotation; therefore, under photo-irradiation, excited dimers contribute to the long-wavelength excimer emission with the efficiency much higher than those for the amorphous blends. Conformation changes in relationship with the degree of molecular rotation are therefore evaluated and identified to assess their influence on the AIE-related fluorescence behaviour.

Acknowledgements

We appreciate the financial support from the National Science Council, Taiwan, under the contract no. NSC 102-2221-E-110-084-MY3 and no. NSC 102-2221-E-110-080.

Notes and references

1 Y. Bae, S. Fukushima, A. Harada and K. Kataoka, *Angew. Chem., Int. Ed.*, 2003, **42**, 4640.
2 H. A. Klok and S. Lecommandoux, *Adv. Mater.*, 2001, **13**, 1217.
3 H. Tang and D. Zhang, *J. Polym. Sci., Part A: Polym. Chem.*, 2010, **48**, 2340.
4 G. J. M. Habraken, C. E. Koning and A. Heise, *J. Polym. Sci., Part A: Polym. Chem.*, 2009, **47**, 6883.
5 C. Robinson and J. C. Ward, *Nature*, 1957, **180**, 1183.
6 S. M. Yu, V. P. Conticello, G. Zhang, C. Kayser, M. J. Fournier, T. L. Mason and D. A. Tirrell, *Nature*, 1997, **389**, 167.
7 K. Tohyama and W. G. Miller, *Nature*, 1981, **289**, 813.
8 S. W. Kuo, H. F. Lee and F. C. Chang, *J. Polym. Sci., Part A: Polym. Chem.*, 2008, **46**, 3108.
9 A. Gitsas, G. Floudas, M. Mondeshki, H. W. Spiess, T. Aliferis, H. Iatrou and N. Hadjichristidis, *Macromolecules*, 2008, **41**, 8072.
10 P. Papadopoulous, G. Floudas, H. A. Klok, I. Schnell and T. Pakula, *Biomacromolecules*, 2004, **5**, 81.
11 S. E. Blondelle, B. Forood, R. A. Houghten and E. Perez-Paya, *Biochemistry*, 1997, **36**, 8393.
12 A. Gitsas, G. Floudas, M. Mondeshki, H. W. Spiess, T. Aliferis, H. Iatrou and N. Hadjichristidis, *Macromolecules*, 2008, **41**, 8072.
13 S. W. Kuo and C. J. Chen, *Macromolecules*, 2011, **44**, 7315.
14 S. W. Kuo and C. J. Chen, *Macromolecules*, 2012, **45**, 2442.
15 Y. S. Lu, Y. C. Lin and S. W. Kuo, *Macromolecules*, 2012, **45**, 6547.
16 P. Doty, J. H. Bradbury and A. M. Holtzer, *J. Am. Chem. Soc.*, 1956, **78**, 947.
17 V. Pokorná, D. Výprachtický and J. Pecka, *Macromol. Biosci.*, 2001, **1**, 185.
18 K. T. Kim, C. Park, G. W. M. Vandermeulen, D. A. Rider, C. Kim, M. A. Winnik and I. Manners, *Angew. Chem.*, 2005, **117**, 8178.
19 L. Rubatat, X. Kong, S. A. Jenekhe, J. Ruokolainen, M. Hojeij and R. Mezzenga, *Macromolecules*, 2008, **41**, 1846.
20 J. Luo, Z. Xie, J. W. Y. Lam, L. Cheng, H. Chen, C. Qiu, H. S. Kwok, X. Zhan, Y. Liu, D. Zhu and B. Z. Tang, *Chem. Commun.*, 2001, 1740.
21 B. Z. Tang, X. Zhan, G. Yu, P. P. S. Lee, Y. Liu and D. Zhu, *J. Mater. Chem.*, 2001, **11**, 2974.
22 *Aggregation-Induced Emission: Fundamentals*, ed. A. Qin and B. Z. Tang, John Wiley & Sons, Ltd, N. Y., 2013.
23 J. Liu, J. W. Y. Lam and B. Z. Tang, *J. Inorg. Organomet. Polym.*, 2009, **19**, 249.
24 Y. Hong, J. W. Y. Lam and B. Z. Tang, *Chem. Commun.*, 2009, 4332.
25 J. Wu, W. Liu, J. Ge, H. Zhang and P. Wang, *Chem. Soc. Rev.*, 2011, **40**, 3483.
26 Y. Hong, J. W. Y. Lam and B. Z. Tang, *Chem. Soc. Rev.*, 2011, **40**, 5361.
27 A. Qin, J. W. Y. Lam and B. Z. Tang, *Prog. Polym. Sci.*, 2012, **37**, 182.
28 J. Chen, C. C. W. Law, J. W. Y. Lam, Y. Dong, S. M. F. Lo, I. D. Williams, D. Zhu and B. Z. Tang, *Chem. Mater.*, 2003, **15**, 1535.
29 B. Z. Tang, Y. Geng, J. W. Y. Lam, B. Li, X. Jing, X. Wang, F. Wang, A. B. Pakhomov and X. Zhang, *Chem. Mater.*, 1999, **11**, 1581.
30 J. Shi, N. Chang, C. Li, J. Mei, C. Deng, X. Luo, Z. Liu, Z. Bo, Y. Q. Dong and B. Z. Tang, *Chem. Commun.*, 2012, **48**, 10675.
31 Y. Liu, X. Tao, F. Wang, J. Shi, J. Sun, W. Yu, Y. Ren, D. Zou and M. Jiang, *J. Phys. Chem. C*, 2007, **111**, 6544.
32 P. Chen, R. Lu, P. Xue, T. Xu, G. Chen and Y. Zhao, *Langmuir*, 2009, **25**, 8395.
33 P. Zhang, H. Wang, H. Liu and M. Li, *Langmuir*, 2010, **26**, 10183.
34 T. H. Kim, M. S. Choi, B. H. Sohn, S. Y. Park, W. S. Lyoo and T. S. Lee, *Chem. Commun.*, 2008, 2364.
35 J. H. Wan, L. Y. Mao, Y. B. Li, Z. F. Li, H. Y. Qiu, C. Wang and G. Q. Lai, *Soft Matter*, 2010, **6**, 3195.
36 M. K. Nayak, *J. Photochem. Photobiol., A*, 2011, **217**, 40.
37 R. H. Chien, C. T. Lai and J. L. Hong, *J. Phys. Chem. C*, 2011, **115**, 12358.
38 R. H. Chien, C. T. Lai and J. L. Hong, *J. Phys. Chem. C*, 2011, **115**, 20732.
39 W. L. Chien, C. M. Yang, T. L. Chen, S. T. Li and J. L. Hong, *RSC Adv.*, 2013, **3**, 6930.
40 S. L. Deng, T. L. Chen, W. L. Chien and J. L. Hong, *J. Mater. Chem. C*, 2014, **2**, 651.
41 S. T. Li, Y. C. Lin, S. W. Kuo, W. T. Chuang and J. L. Hong, *Polym. Chem.*, 2012, **3**, 2393.
42 R. K. Scheule, F. Cardinaux, G. T. Taylor and H. A. Scheraga, *Macromolecules*, 1976, **9**, 23.
43 P. Pasman, F. Rob and J. W. Verhoeven, *J. Am. Chem. Soc.*, 1982, **104**(19), 5127–5133.
44 X. G. Chen, R. Schweitzer-Stenner, S. A. Asher, N. G. Mirkin and S. Krimm, *J. Phys. Chem. B*, 1995, **99**, 3074.
45 R. Schweitzer-Stenner, G. Sieler, N. G. Mirkin and S. Krimm, *J. Phys. Chem. A*, 1998, **102**, 118.
46 S. W. Kuo, P. H. Tung and F. C. Chang, *Macromolecules*, 2006, **39**, 9388.
47 S. W. Kuo, C. L. Lin and F. C. Chang, *Polymer*, 2002, **43**, 3943.
48 A. Sanchez-Ferrer and R. Mezzenga, *Macromolecules*, 2010, **43**, 1093.
49 Y. E. Khoury, R. Hielscher, M. Voicescu, J. Gross and P. Hellwig, *Vib. Spectrosc.*, 2011, **55**, 258.
50 K. Murata, E. Katoh, S. Kuroki and I. Ando, *J. Mol. Struct.*, 2004, **689**, 223.
51 H. R. Kricheldorf and D. Muller, *Macromolecules*, 1983, **16**, 615.
52 C. M. Yang, I. W. Lee, T. L. Chen, W. L. Chien and J. L. Hong, *J. Mater. Chem. C*, 2013, **1**, 2842.
53 X. Luo, J. Li, C. Li, L. Heng, Y. Q. Dong, Z. Liu, Z. Bo and B. Z. Tang, *Adv. Mater.*, 2011, **23**, 3261.

